Data Repository Item 2009003

"An abrupt transition from magma-starved to magma-rich rifting in the eastern Black Sea"
Donna J. Shillington, Caroline L. Scott, Timothy A. Minshull, Rosemary A. Edwards, Peter J. Brown, and Nicky White

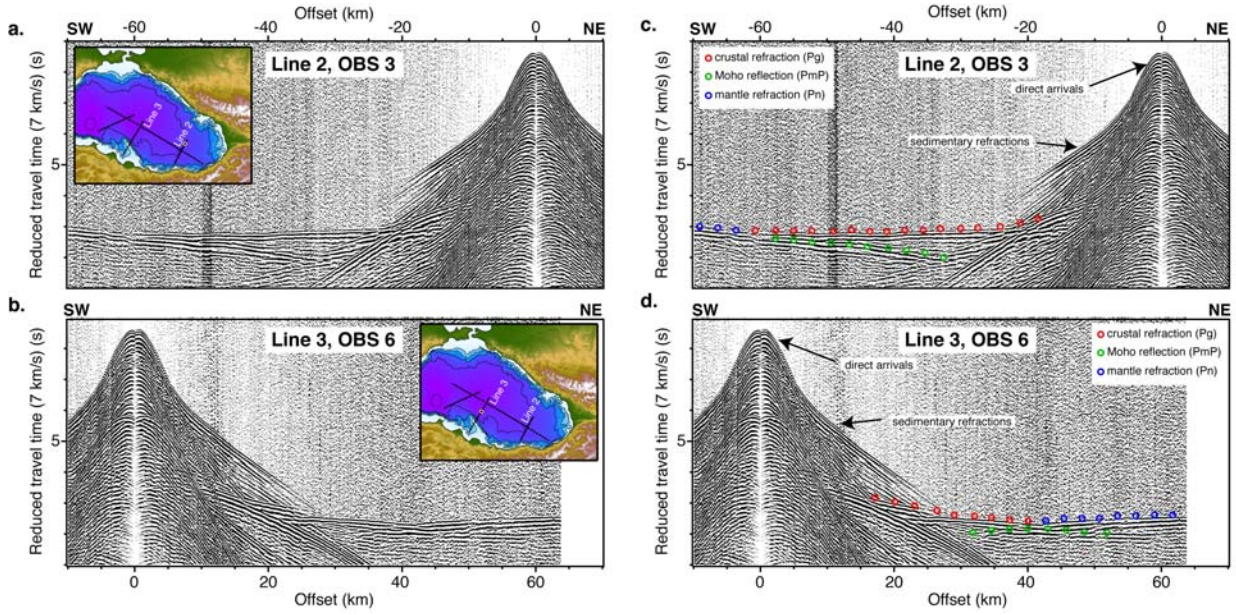

Figure DR1: Examples of wide-angle seismic refraction data recorded on interpreted thick oceanic crust on Line 2 (a and c) and thinned continental crust on Line 3 (b and d). The vertical component of the geophone is shown for both instruments. The x-axis represents the distance between the OBS and the seismic source, and the y-axis indicates reduced travel time, which causes phases with an apparent velocity of 7 km/s to appear flat. Figures a and b show records from each OBS without interpretations; and c and d show interpreted crustal refractions (Pg, red), reflections from the crust-mantle boundary (PmP, green) and mantle refractions (Pn, blue). Note that crustal refractions occur as first arrivals over a larger range of offsets on Line 2 than Line 3, indicating a thicker crust is present beneath Line 2. Additionally, crustal refractions on Line 2 have higher apparent velocities than on Line 3, which indicates that the crust beneath Line 2 also has higher velocities.

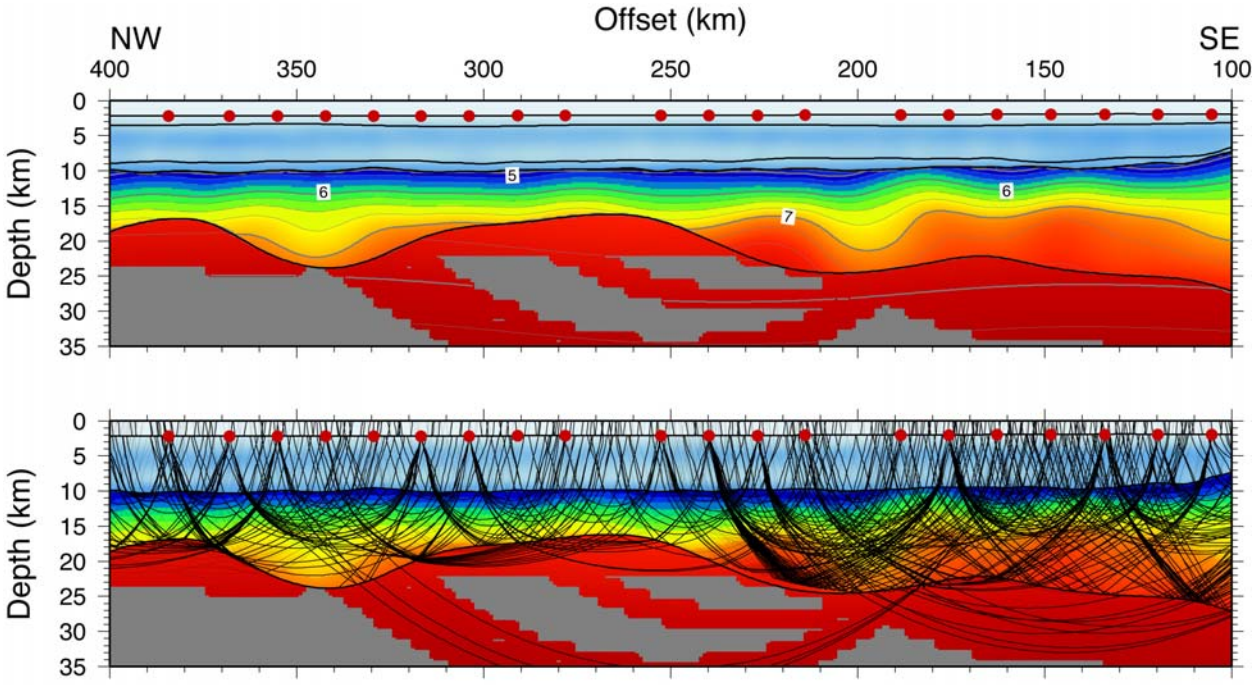

Figure DR2. Velocity model and ray coverage in the crust and mantle along Line 1. Velocities greater than 4.0 km/s are contoured every 0.25 km/s in the upper panel. Every 13th ray is plotted in the lower panel. This model was based on 31,574 picks and has a chi-squared (misfit weighted by uncertainty) of 1.44.

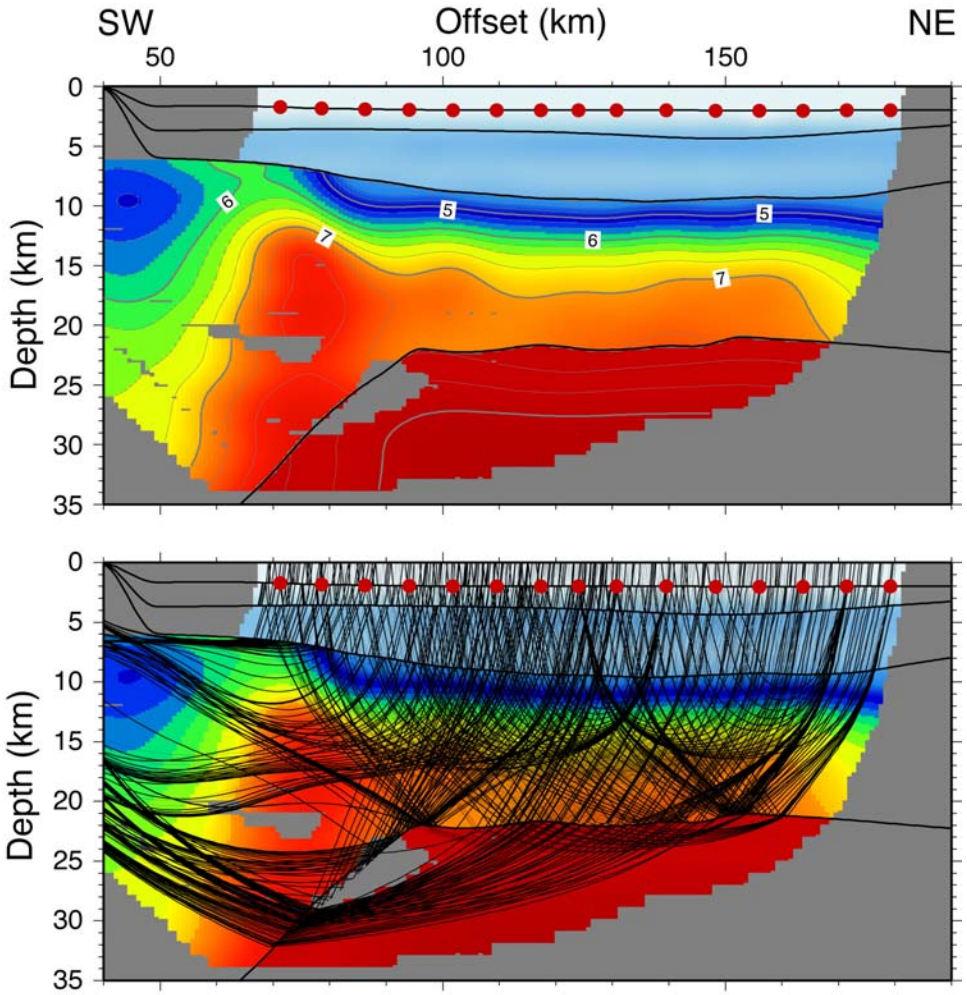

Figure DR3. Velocity model and ray coverage in the crust and mantle along Line 2. Velocities greater than 4.0 km/s are contoured every 0.25 km/s in the upper panel. Every 19th ray is plotted in the lower panel. This model was based on 106,546 picks and has a chi-squared (misfit weighted by uncertainty) of 1.08.

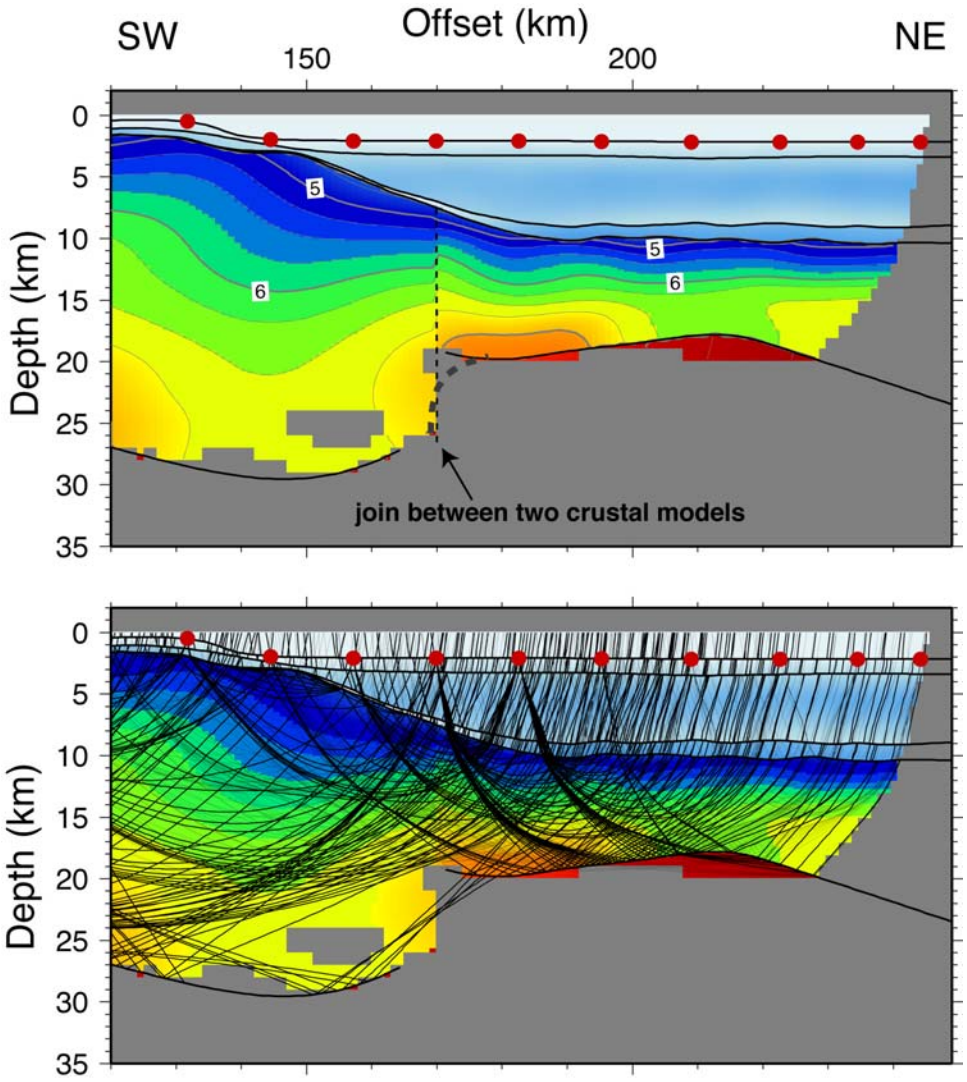

Figure DR4. Velocity model and ray coverage in the crust and mantle along Line 3. Velocities greater than 4.0 km/s are contoured every 0.25 km/s in the upper panel. Every 13th ray is plotted in the lower panel. This model was based on 40,561 picks and has a chi-squared (misfit weighted by uncertainty) of 1.28. Crustal velocity structure was modeled in two parts, and the two models are joined at model km 170, causing the kink in velocity contours. We modeled this line in two parts because earlier velocity models created by first-arrival tomography indicated an abrupt change in crustal thickness occurs at ~170 km. Such abrupt variations in crustal thickness can produce two PmP reflections at the same source-receiver offset (e.g., Van Avendonk et al., in press). When two reflections are produced at the same source-receiver offset, the tomographic algorithm employed in this study (Jive3D) will compare the observed travel time with the earliest predicted travel time (Hobro et al., 2003). As a result, it could not recover a steep Moho. Therefore we decided to model this profile in two parts. In the landward section, we modeled the deeper Moho reflections (when two reflection were present). In the seaward section, we modeled the shallower Moho reflection (when two reflections were present). The approximate location of the Moho between 160-180 km is based on the results of first-arrival tomography (dashed grey line).

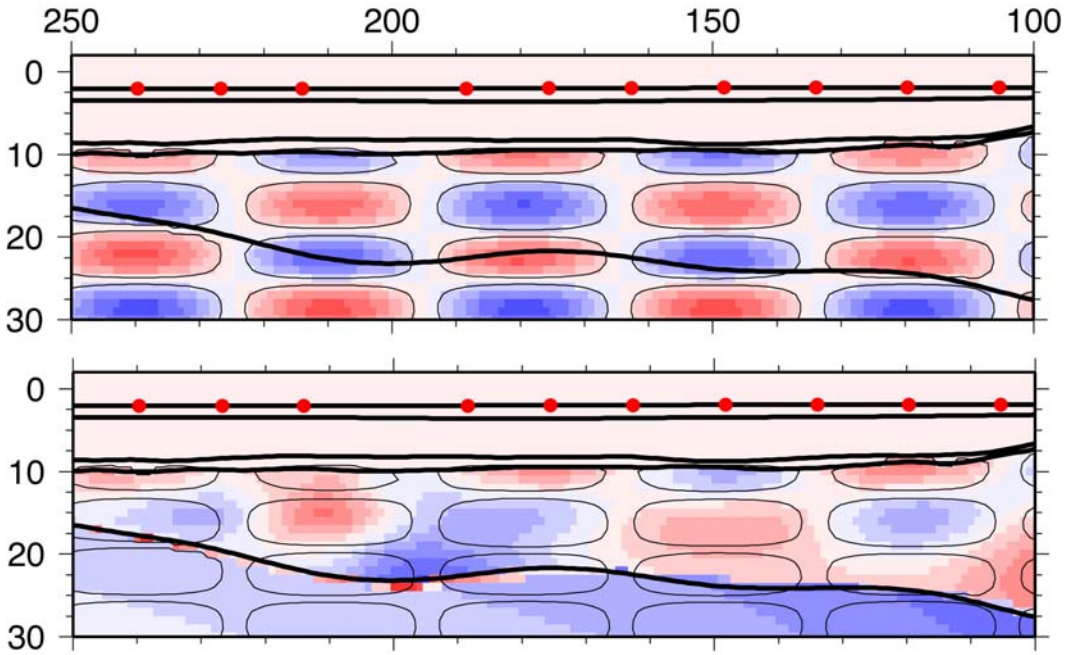

Figure DR5. Checkerboard test of Line 1 in the vicinity of the transition between thinned continental crust without synrift magmatism and magmatically robust oceanic crust. **a.** Input checkerboard. The checks have dimensions of 30x6 km and represent 5% velocity anomalies. The black lines indicate ± 0.1 km/s contours. This pattern of positive and negative velocity anomalies were superimposed on the final velocity model of Line 1, and rays were traced through this model to create synthetic travel times. We added random noise to these synthetic travel times and inverted them for velocity structure. The recovery of anomalies with various dimensions is an approximate indication of the scale lengths of features that can be resolved. **b.** Recovery of checkerboard. The black lines indicate ± 0.1 km/s contours from **a**. for reference, while the colored panel shows the recovered velocity anomalies. Note that most checks are recovered in the upper and middle crust, but are not as well resolved in the lowermost crust, whose velocity is not constrained by refractions. This suggests that features of this scale length can be resolved with our inversion. Features with comparable or larger dimensions are the basis for our interpretation and conceptual model.

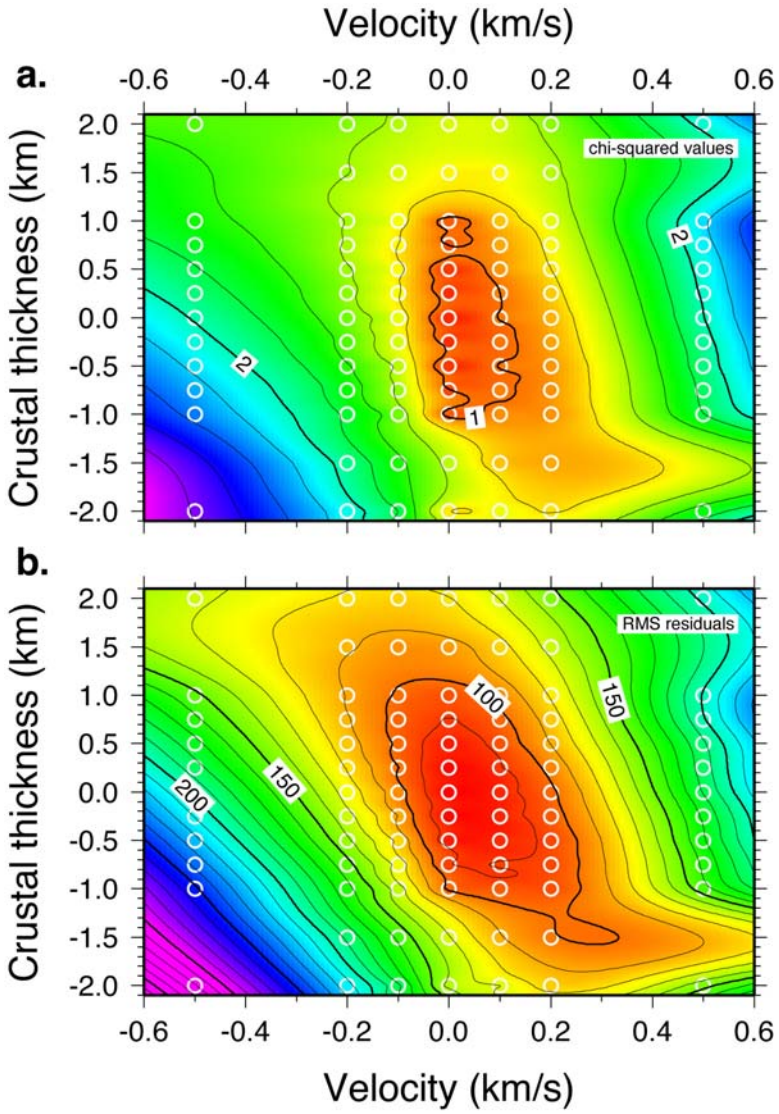

Figure DR6 a. Gridded and contoured chi-squared values (misfit weighted by uncertainty) for arrivals constraining the seaward portion of the model as a function of variations in crustal thickness and lower crustal velocity for Line 2. We varied the crustal thickness and the velocities in the lower crust below 18 km in our final velocity model, traced rays through this model, and calculated the data misfit. Velocities were only varied below 18 km because this is the deepest portion of the crust constrained by refractions (Fig. DR3). Contoured at 0.1. Colored dots with white outlines show the changes in crustal thickness and lower crustal velocity for which data misfit was calculated. **b.** Gridded and contoured RMS residuals for variations in crustal thickness and lower crustal velocity. Generated in the same way as described above. Contoured every 10 ms. Colored dots with white outlines show the changes in crustal thickness and lower crustal velocity for which data misfit was calculated. Both figures show that there is a relatively small tradeoff between velocity and crustal thickness (note the positive correlation). They indicate that our crustal thickness can be constrained within approximately ±1 km, and lower crustal velocities can be constrained within approximately ±0.1 km/s. Even if the maximum uncertainties are applied to the crustal structure of all lines, a significant along-strike change in lower crustal velocity and crustal thickness is still required by the data.

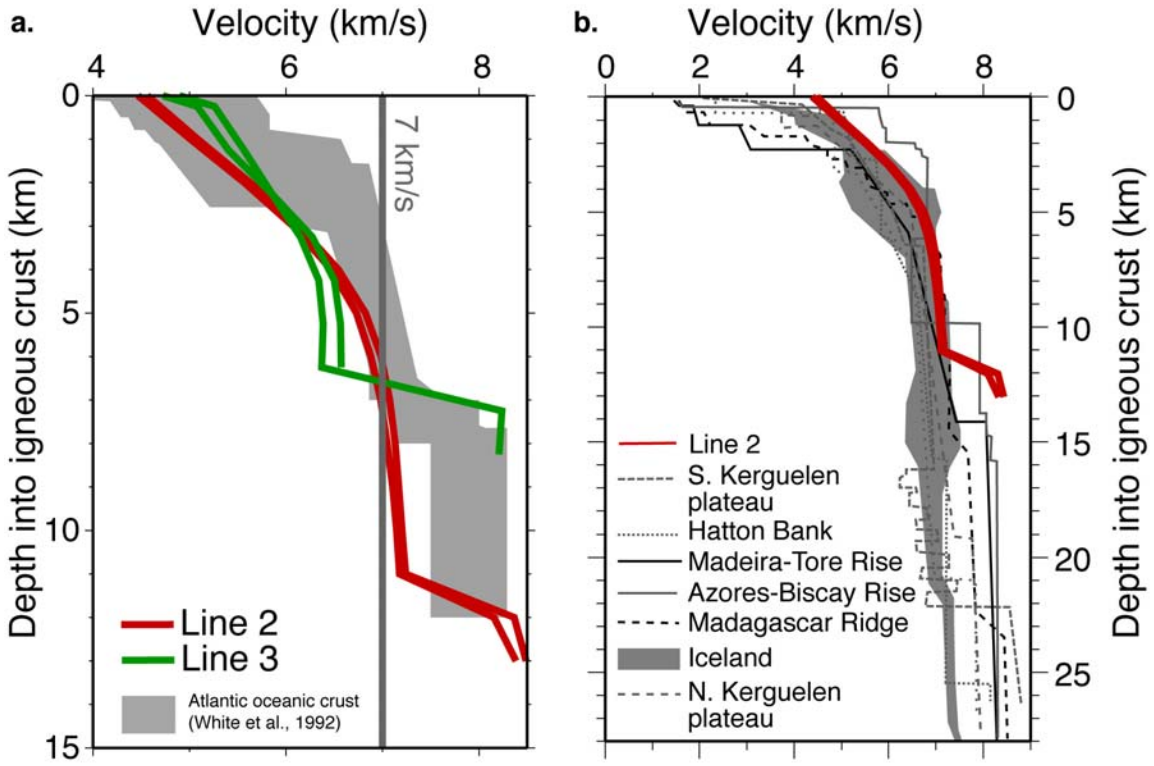

Figure DR7 a. 1D velocity profiles taken from 123 km and 147 km on Line 2 (red) and from 210 and 220 km on Line 3 (green). Velocity structure associated with Atlantic oceanic crust (grey shaded region) from compilation of White et al (1992) is shown for comparison. Dark grey line indicates 7 km/s for reference. Note that the maximum lower crustal velocities from Line 3 (~6.6 km/s) are lower than those of Atlantic lower oceanic crust. Additionally, Line 3 does not exhibit a high velocity gradient in the upper crust, which is commonly associated with Layer 2 in oceanic crust. For these reasons, we interpret crust along this profile as thinned continental crust. The crustal structure along Line 2 is different from Line 3; the crust is much thicker and has higher lower crustal velocities (7.0-7.2 km/s). A high velocity gradient is associated with the upper crust, and a low velocity gradient is associated with the lower crust. This is characteristic of oceanic crust. However, the crust along Line 2 is clearly much thicker than 'normal' oceanic crust. **b**. Comparison between 1D profiles from Line 2 (red, taken from the same locations as in Fig. DR7a) and profiles from oceanic crust near volcanic rifted margins and oceanic plateaux (grey and black lines) compiled by Minshull (2002). The velocity structure of Line 2 closely resembles that of these provinces. Based on these arguments, we suggest that the crust along Line 2 is thick oceanic crust produced in the presence of a mantle thermal or composition anomaly. However, we note that it could also be interpreted as highly thinned continental crust with significant magmatic addition. In either case, an abrupt along-strike change in magmatism is required and our conceptual model applies.

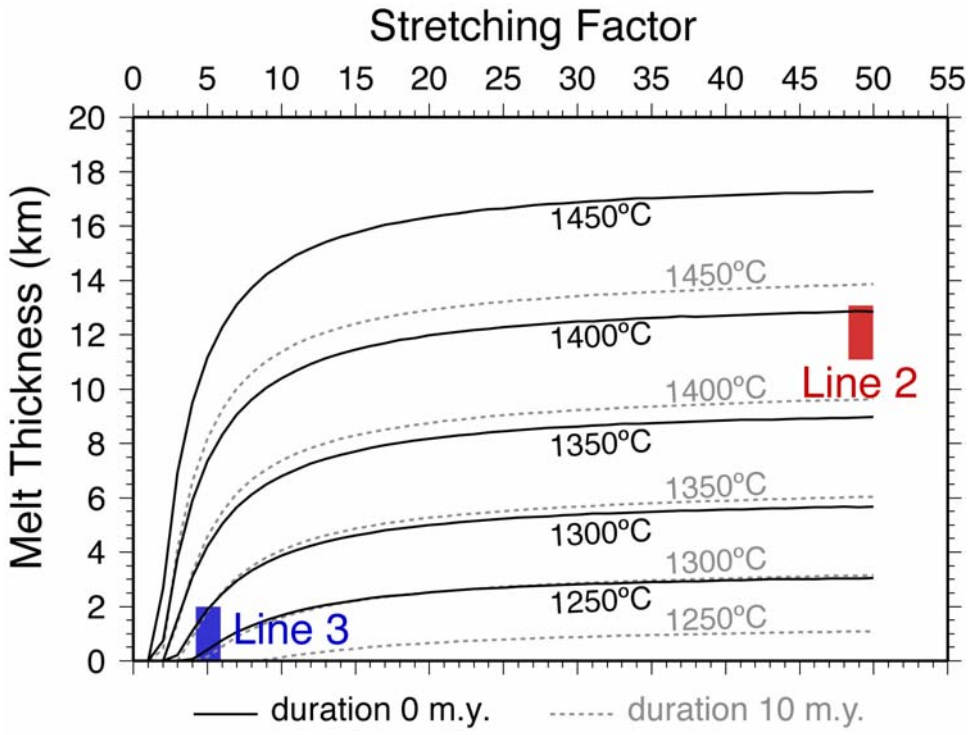

Figure DR8. Melt thickness predictions calculated using method of Bown and White (1995). Thick lines show predicted relationship between stretching factor (initial/final crustal thickness) and melt thickness based on batch melting of anhydrous peridotite for instantaneous rifting. Dotted grey lines are calculated using a rift duration of 10 m.y. Longer rift durations result in less melt because there is more time for conductive cooling during rifting, which suppresses magmatism. A stretching factor of 50 and instantaneous rifting approximate seafloor spreading. In the absence of other factors, a temperature difference of ~150ºC is required to explain the difference in melt thickness between Lines 2 and 3.

References Cited

Bown, J.W., and White, R.S., 1995, Effect of finite extension rate on melt generation at rifted continental margins: J. Geophys. Res., v. 100, p. 18,011-18,029.

Hobro, J.W.D., Singh, S.C., and Minshull, T.A., 2003, Three-dimensional tomographic inversion of combined reflection and refraction seismic traveltime data: Geophys. J. Int., v. 152, p. 79-93.

Minshull, T.A., 2002, Seismic Structure of the Oceanic Crust and Passive Continental Margins, International Handbook of Earthquake and Engineering Seismology, Volume 81A, Intl. Assoc. Seismol. & Phys. Earth's Interior, Committee on Education.

Van Avendonk, H.J.A., Lavier, L., Shillington, D.J., and Manatschal, G., in press, Extension of continental crust at the margin of the eastern Grand Banks, Newfoundland: Tectonophysics, p. doi:10.1016/j.tecto.2008.05.030.

White, R.S., McKenzie, D., and O'Nions, R.K., 1992, Oceanic Crustal Thickness From Seismic Measurements and Rare Earth Element Inversions: J. Geophys. Res., v. 97, p. 19,683-19,715.